REGULAR ARTICLE

blood advances

Enhanced engraftment of human myelofibrosis stem and progenitor cells in MISTRG mice

Veronika Lysenko,[1] Nicole Wildner-Verhey van Wijk,[1] Kathrin Zimmermann,[1] Marie-Christine Weller,[1] Marco Bühler,[2] Mattheus H. E. Wildschut,[1,3] Patrick Schürch,[1] Christine Fritz,[2] Ulrich Wagner,[2] Laura Calabresi,[4] Bethan Psaila,[5-7] Richard A. Flavell,[8] Alessandro M. Vannucchi,[4] Adam J. Mead,[5-7] Peter J. Wild,[9] Stefan Dirnhofer,[10] Markus G. Manz,[1,*] and Alexandre P. A. Theocharides[1,*]

[1]Department of Medical Oncology and Hematology, University of Zurich and University Hospital Zurich, Zurich, Switzerland; [2]Institute of Pathology and Molecular Pathology, University Hospital Zurich, Zurich, Switzerland; [3]Institute of Molecular Systems Biology, ETH Zurich, Zurich, Switzerland; [4]Center for Research and Innovation of Myeloproliferative Neoplasms, Azienda Ospedaliero, Universitaria Careggi, University of Florence, Florence, Italy; [5]Haematopoietic Stem Cell Biology Laboratory, Medical Research Council Weatherall Institute of Molecular Medicine, [6]Medical Research Council Molecular Haematology Unit, Weatherall Institute of Molecular Medicine, and [7]National Institute for Health Research Biomedical Research Centre, University of Oxford, Oxford, United Kingdom; [8]Department of Immunobiology, Yale University, New Haven, CT; [9]Dr. Senckenberg Institute of Pathology, University Hospital Frankfurt, Frankfurt, Germany; and [10]Institute of Pathology, University Hospital, University of Basel, Basel, Switzerland.

Key points

- Human myelofibrosis stem and progenitor cells efficiently engraft in humanized MISTRG mice independent of risk category and disease stage.
- The clonal architecture of myelofibrosis is maintained in MISTRG patient-derived xenografts.

The engraftment potential of myeloproliferative neoplasms in immunodeficient mice is low. We hypothesized that the physiological expression of human cytokines (macrophage colony-stimulating factor, interleukin-3, granulocyte-macrophage colony-stimulating factor, and thrombopoietin) combined with human signal regulatory protein α expression in *Rag2*$^{-/-}$*Il2rγ*$^{-/-}$ (MISTRG) mice might provide a supportive microenvironment for the development and maintenance of hematopoietic stem and progenitor cells (HSPC) from patients with primary, post–polycythemia or post–essential thrombocythemia myelofibrosis (MF). We show that MISTRG mice, in contrast to standard immunodeficient NOD.*Cg-Prkdc*^{scid}*Il2rg*^{tm1Wjl}/SzJ and *Rag2*$^{-/-}$*Il2rγ*$^{-/-}$ mice, supported engraftment of all patient samples investigated independent of MF disease stage or risk category. Moreover, MISTRG mice exhibited significantly higher human MF engraftment levels in the bone marrow, peripheral blood, and spleen and supported secondary repopulation. Bone marrow fibrosis development was limited to 3 of 14 patient samples investigated in MISTRG mice. Disease-driving mutations were identified in all xenografts, and targeted sequencing revealed maintenance of the primary patient sample clonal composition in 7 of 8 cases. Treatment of engrafted mice with the current standard-of-care Janus kinase inhibitor ruxolitinib led to a reduction in human chimerism. In conclusion, the established MF patient-derived xenograft model supports robust engraftment of MF HSPCs and maintains the genetic complexity observed in patients. The model is suited for further testing of novel therapeutic agents to expedite their transition into clinical trials.

Introduction

Myelofibrosis (MF) is a myeloproliferative neoplasm (MPN) occurring mostly in the elderly population that is either primarily diagnosed or evolves after the initial diagnosis of polycythemia vera or essential thrombocythemia. MF is characterized by an expansion of the myeloid and megakaryocytic lineages, followed by a steady deposition of fibers in the bone marrow (BM) and subsequent extramedullary hematopoiesis.[1] Patients with MF have a poor life expectancy, suffer from severe constitutional

Submitted 17 December 2019; accepted 28 April 2020; published online 5 June 2020. DOI 10.1182/bloodadvances.2019001364.

*M.G.M. and A.P.A.T. contributed equally to this study.

For original data, protocols, and reagents, please contact the corresponding author, Alexandre P. A. Theocharides (alexandre.theocharides@usz.ch).

The full-text version of this article contains a data supplement.

symptoms, and have a 10% to 20% lifetime risk of leukemic transformation.[2,3] In the majority of patients, MF originates from a hematopoietic stem cell (HSC) that acquires a driver mutation in 1 of 3 genes: Janus kinase 2 (*JAK2*), calreticulin (*CALR*), or the thrombopoietin receptor (*MPL*).[4-10] Additionally, prior or later acquired mutations in epigenetic modifiers and the spliceosome complex are associated with an increased risk of leukemic transformation and reduced survival.[11] All 3 driver mutations lead to cytokine-independent activation of JAK-STAT signaling, and patients carrying any of the 3 mutations in their MF clones respond to JAK inhibitor (JAKi) therapy.[12] Although JAKi relieve MF symptoms and reduce spleen (SPL) size, the MF clone persists in most cases, and the only curative therapy for MF remains allogeneic HSC transplantation (allo-HSCT).[13,14] For this reason, there is a need for therapeutic improvements and for respective suitable models to test new therapies with disease-modifying potential.

Although multiple MPN mouse models that carry one of the driver mutations mimic MF, these models do not reflect the heterogeneity observed in patients.[15] Patient-derived xenograft (PDX) models have emerged as powerful tools to investigate normal and malignant hematopoiesis in an individual patient-based approach.[16] However, engraftment of less-aggressive malignancies, like MF, remains limited despite various efforts.[17-19] Transplantation of human peripheral blood or splenic MF CD34$^+$ cells into adult NOD.*Cg-Prkdc^{scid} Il2rg^{tm1Wjl}*/SzJ (NSG) mice resulted in low-level multilineage engraftment that did not reflect the myeloid character of MF.[17] Injection into implanted human mesenchymal stem cell–derived ossicles generated a transient human graft that diminished significantly over time.[19]

Previously we developed next-generation humanized mice to substitute for non-cross–reactivity of mouse cytokines to human hematopoietic stem and progenitor cells (HSPCs) and myeloid cells.[20,21] These mice were modified to express human macrophage colony–stimulating factor (*M-CSF*), interleukin-3 (*IL-3*), granulocyte-macrophage colony–stimulating factor (*GM-CSF*), signal regulatory protein α (*SIRPα*), and thrombopoietin on the *Rag2$^{-/-}$Il2rγ$^{-/-}$* mouse background (abbreviated "MISTRG"). In particular, the interaction between human CD47 and SIRPα on mouse macrophages is essential to allow the development of human hematopoiesis in mice.[22] In prior studies, we demonstrated that MISTRG mice efficiently engraft favorable-risk acute myeloid leukemia (AML) and myelodysplastic syndrome (MDS), which develop poorly in standard immunodeficient mice (NSG).[23,24] In this study, we show that MISTRG mice provide a supportive environment for MF development in comparison with NSG mice.

Materials and methods

Patient material and samples

Peripheral blood (PB) was collected from 14 MF patients (Table 1) after obtaining informed consent. The study was approved by the local ethics committee (KEK-ZH-NR: 2009-0062/1 and BASEC-NR: 2018-00539). MF diagnoses were made according to the World Health Organization (WHO) 2016 classification. HSPC (CD34$^+$) cells were purified from the PB of MF patients using Ficoll density gradient centrifugation followed by isolation with the MACS CD34 MicroBead Kit (Miltenyi Biotec; supplemental Table 1). MF CD34$^+$ cells were cryopreserved in fetal calf serum (FCS) and 10% dimethyl sulfoxide. Before xenotransplantation, the cells were slowly thawed in Iscove modified Dulbecco medium 50% FCS at 37°C and resuspended in 25 μl of phosphate-buffered saline for injection.

Mice

MISTRG mice were generated as previously described and expressed knock-in replacement of mouse *M-csf*, *Il-3*, *Gm-csf*, *Sirpα*, and *Tpo* by its human ortholog on the *Rag2$^{-/-}$Il2rγ$^{-/-}$* background.[20,21,23,25] *Rag2$^{-/-}$Il2rγ$^{-/-}$* mice on the BALB/c background were bred and maintained at the University Hospital Zurich animal facility. NSG mice were obtained from the Jackson Laboratory. Mice were retained at the University Hospital Zurich animal facility in accordance with the Swiss Federal Veterinary office. Animal experiments were approved by the cantonal veterinary office of Zurich, Switzerland.

Xenotransplantation

Newborn *Rag2$^{-/-}$Il2rγ$^{-/-}$*, NSG, and MISTRG mice were sublethally irradiated (X-ray irradiation with RS-2000 irradiator; Rad Source) with 1 × 150 cGy and transplanted using a 22-gauge needle (Hamilton Company) intrahepatically with cryopreserved PB-purified CD34$^+$ cells from MF patients. Intrahepatic injections were performed by injecting 25 μL of cell suspension per newborn mouse. The number of cells injected ranged from 1.95×10^5 to 1.05×10^6 per recipient mouse (supplemental Table 2). For each patient sample, the same cell number was injected into NSG and MISTRG mice. Mice were euthanized ≥16 weeks after transplantation or when sick (range, 3.6 to 19.7 weeks). For secondary transplantations, newborn NSG and MISTRG mice were sublethally irradiated with 1 × 150 cGy and then transplanted as described above with human CD45$^+$ cells purified from primary animals using a BD FACSAria II sorter. The ratio of primary to secondary recipients was 2:1 (patient 10), 2:3 (patient 11), and 1:2 (patient 13) (Figure 4; supplemental Table 3). Mice were analyzed ≥16 weeks after transplantation or when sick (range, 17.1 to 17.9 weeks).

Engraftment assessment by flow cytometry

Cells were isolated from the BM, PB, and SPL of euthanized animals upon primary and secondary transplantation, and stained with the following monoclonal antibodies to determine human cell reconstitution: Pacific blue–conjugated anti-human CD45 (clone HI30, eBioscience), fluorescein isothiocyanate (FITC)–conjugated anti-human CD38 (clone HIT2, BD Pharmingen), phycoerythrin (PE)/Cy7-conjugated anti-human CD34 (clone 8G12, BD Pharmingen), PE-conjugated anti-human CD19 (clone SJ25C1, eBioscience), allophycocyanin (APC)/Cy7-conjugated anti-human CD14 (clone M5E2, Biolegend), APC-conjugated anti-human CD33 (clone WM53, BD Pharmingen), and PE/Cy5-conjugated anti-mouse CD45 (clone 30-F11, eBioscience). Stained cells were acquired on a BD LSRFortessa cell analyzer. Human engraftment was defined as ≥1% human CD45$^+$ cells out of all cells.

Histology and immunohistochemistry

Tibias were isolated from mice, fixed in 4% phosphate-buffered formalin, and then embedded in paraffin. Tissue sections (4 μm) were stained with hematoxylin and eosin (H&E) for conventional morphology and with Gömöri for the quantification and distribution of reticulin fibers. Immunohistochemistry was performed on serial tissue sections using an automated immunostainer, Benchmark XT (Roche/Ventana, Tucson, AZ), according to routine standard operation procedures. The streptavidin–biotin

Table 1. Characteristics of MF patients

PID	Diagnosis	Stage	Driver	NGS	PB blasts, %	MIPSS70	MYSEC	Therapy	Follow-up
1	PMF	Chronic	CALR	MPL	1.5	IM	—	INF	Alive (CP)
2	PMF	Chronic	CALR	ASXL1, U2AF1	1.5	High	—	Rux	Alive (AP)
3	PMF	Accelerated	JAK2	ASXL1	18.5	High	—	Rux	Dead (post-allo)
4	PMF	Accelerated	None	ASXL1, NRAS, SETBP1, SRSF2	11	High	—	Rux	Dead (AML)
5	PMF	Accelerated	JAK2	ASXL1, KRAS, TET2, U2AF1	17.5	High	—	Rux	Dead (AML)
6	PPV-MF	Chronic	JAK2	ASXL1, SF3B1	8.5	—	IM2	Rux	Alive (CP)
7	PPV-MF	Chronic	JAK2	SF3B1	13.5	—	High	Rux*	Dead (AP)
8	PPV-MF	Accelerated	JAK2	EZH2, PHF6	14	—	High	Rux	Dead (BM failure)
9	PET-MF	Chronic	CALR	ASXL1, GATA2, TET2	0.5	—	IM2	Rux	Alive (CP)
10	PET-MF	Chronic	CALR	SF3B1	0.5	—	Low	None	Alive (CP)
11	PET-MF	Chronic	CALR	TET2	0.5	—	IM1	ANA	Alive (CP)
12	PET-MF	Chronic	CALR	ASXL1	2	—	IM1	Rux	Alive (CP)
13	PET-MF	Chronic	JAK2	ASXL1, RUNX1, SRSF2, TET2, TP53	6	—	High	Rux	Dead (AP)
14	PET-MF	Accelerated	CALR	ASXL1, TET2	8	—	IM1	Rux	Alive (allo)

Allo, allo-HSCT; AML, acute myeloid leukemia; ANA, anagrelide; AP, accelerated phase; CP, chronic phase; IM, intermediate; INF, pegylated interferon α-2a; MIPSS70, mutation-enhanced international prognostic scoring system for PMF; MYSEC, MF secondary to PV and ET-prognostic model; NGS, next-generation sequencing performed on whole PB or BM; PET-MF, post–essential thrombocythemia MF; PID, patient identification number; PMF, primary MF; PPV-MF, post–polycythemia vera MF.

*Treatment was stopped before sampling.

peroxidase technique with aminoethylcarbazole as chromogen was applied. The following antibodies were used for immunohistochemistry: CD45 (clone RP2/18, prediluted; Roche/Ventana), CD33 (clone SP266, prediluted; Roche/Ventana), CD61 (clone 2f2, prediluted; Roche/Ventana), CD14 (clone SP192, prediluted; Spring Bioscience), and CD15 (clone Carb-3, prediluted; DAKO).

DNA isolation

Erythrocyte lysis was performed on BM and/or PB leukocytes were subjected to DNA extraction using the QIAamp DNA Blood Mini Kit (Qiagen). DNA was quantified using the Qubit dsDNA HS Assay Kit (ThermoFisher Scientific), according to the manufacturer's instructions. DNA from frozen PDX BM was extracted using the QIAamp DNA Mini Kit (Qiagen).

Targeted sequencing

Analysis of somatic gene mutations was performed by targeted Next Generation Sequencing using the TruSight myeloid sequencing panel (Illumina, San Diego, CA). The panel covers the full coding sequence of 15 genes (*BCOR*, *BCORL1*, *CDKN2A*, *CEBPA*, *CUX1*, *DNMT3A*, *ETV6/TEL*, *EZH2*, *IKZF1*, *KDM6A*, *PHF6*, *RAD21*, *RUNX1*, *STAG2*, *ZRSR2*) and exonic hot spot regions of 39 genes (*ABL1*, *ASXL1*, *ATRX*, *BRAF*, *CALR*, *CBL*, *CBLB*, *CBLC*, *CSF3R*, *FBXW7*, *FLT3*, *GATA1*, *GATA2*, *GNAS*, *HRAS*, *IDH1*, *IDH2*, *JAK2*, *JAK3*, *KIT*, *KRAS*, *MLL*, *MPL*, *MYD68*, *NOTCH1*, *NPM1*, *NRAS*, *PDGFRA*, *PTEN*, *PTPN11*, *SETBP1*, *SF3B1*, *SMC1A*, *SMC3*, *SRSF2*, *TET2*, *TP53*, *U2AF1*, *WT1*). Libraries were prepared according to the manufacturer's protocol using 150 ng of genomic DNA (gDNA) isolated from the BM aspirate, the PB, or purified $CD34^+$ from patient samples and DNA isolated from the whole BM of their respective PDX samples. For PDX samples, the endpoint DNA concentration was calculated based on the percentage of human $CD45^+$ cells out of all cells. The panel oligo pool was hybridized to gDNA and unbound oligos were removed using a size-selection filter. A subsequent extension-ligation reaction resulted in products containing the targeted regions of interest. These products were amplified using primers that add index sequences as well as adapters required for cluster generation. PCR products were purified using Agencourt AMPure XP magnetic beads (Beckman Coulter). Libraries were normalized to ensure equal library representation. Equal volumes of each library were combined, heat denatured, and spiked with 1% 20 pM PhiX control for sequencing. Paired end sequencing was performed using the MiSeq Reagent Kit V3 (600 cycles) on the MiSeq sequencing platform or the NextSeq 500/550 Mid Output Kit V2 (300 cycles) on the NextSeq platform (Illumina). Data processing and analysis in respect to single-nucleotide variants was performed using the Illumina BaseSpace pipeline (v3.0.0.0; Illumina) based on the human genome reference hg19. For the initial detection of variants, we filtered out those mutations that did not show a variant allele frequency (VAF) ≥5%, a minimum average base quality of Q20 and a coverage of at least 500 at the specific location. When variants were detected in the patient sample, but not in the PDX or vice versa, we used integrative genomic viewer to identify these variants with a sensitivity of ≥1% in PDX or in the respective patient sample. For the analysis of large insertions and deletions (eg, CALR mutation type 1), data were mapped to hg19 using Burrows-Wheeler Aligner with Maximal Exact Matches. Indel detection was performed using Pindel and Scalpel, which allow an estimation of the VAFs based on the number of mutant reads and total reads at the specific location. To rule out that reads originating from mouse with high similarity to reads originating from human xenografts might be wrongly aligned to hg19 and thus distort the apparent variant allele frequencies, we aligned all reads to an artificial reference comprised of a combination of complete human (hg19) and mouse (mm10) reference genome sequences as described.[24,26]

Treatment with ruxolitinib (Rux)

Rux [β-cyclopentyl-4-(7H-pyrrolo[2,3-d]pyrimidin-4-yl)-(Betar)-1H-pyrazole-1-propanenitrile, phosphate] was purchased from

Sigma-Aldrich and freshly reconstituted in 0.5% hydroxypropyl methylcellulose (Sigma-Aldrich) every 4 days. MISTRG mice that engrafted were distributed into 2 groups, and either Rux (90 mg/kg BID) or vehicle was administered by oral gavage twice a day for 21 consecutive days. Mice that received vehicle treatment were given 0.5% hydroxypropyl methylcellulose without the compound. After the treatment, mice were euthanized, and further analysis of PB and organs was performed. Complete blood counts were performed on a Siemens ADVIA 2120.

Statistical analysis

All statistical analyses were performed in GraphPad Prism 8 using either the 2-tailed unpaired Student *t* test when the data followed a Gaussian distribution or the Mann-Whitney *U* test when it was from a non-Gaussian distribution (not significant; $*P < .05$; $**P < .01$; $***P < .001$; $****P < .0001$).

Results

We postulated that the expression of human cytokines and SIRPα in MISTRG mice might foster the engraftment and maintenance of MF HSPCs and the differentiation of mature MF hematopoietic cells. We accessed a publicly available database to assess the expression of the respective receptors in PB granulocytes of 18 MF patients compared with 11 healthy age-matched donors (supplemental Figure 1).[27] Indeed, the expression of the IL-3 receptor (IL3RA, $P = .0031$), the GM-CSF receptor (CSF2RA, $P < .0001$), and CD47 ($P < .0001$) was elevated on MF granulocytes, indicating the possibility that the presence of these human cytokines and the interaction between CD47 and SIRPα might be supportive for human MF cell engraftment in vivo. Consequently, we transplanted $CD34^+$ PB cells from 14 MF patients into sublethally irradiated newborn MISTRG mice and used NSG mice as controls (Table 1; Figure 1A). In addition, 2 MF patient samples were transplanted into *Rag2*$^{-/-}$*Il2rγ*$^{-/-}$ mice, which neither express human cytokines nor human SIRPα (supplemental Figure 2). At the time of sample donation, 10 of 14 patients (71%) were receiving treatment with the JAKi Rux. The total median human engraftment ($CD45^+$) was significantly higher in the BM (26.50% vs 2.75%; $P < .001$), the PB (51.70% vs 0.44%; $P < .0001$), and the SPL (5.30% vs 0.16%; $P < .0001$) of MISTRG compared with NSG mice (Figure 1B-C). Human MF engraftment was not observed in *Rag2*$^{-/-}$*Il2rγ*$^{-/-}$ mice. All MISTRG mice (49 of 49, 100%) in comparison with only 60% of NSG mice (24 of 40) showed ≥1% human engraftment in the BM. Importantly, human BM engraftment of ≥10%, which would allow robust assessment of candidate compounds in vivo, was noted in 90% (44 of 49) of MISTRG mice compared with 33% (13 of 40) of NSG mice (Figure 1C). The superior engraftment observed in MISTRG mice was independent of MF risk categories (dynamic international prognostic scoring system [DIPSS], mutation-enhanced international prognostic scoring system for PMF [MIPSS70], and MF secondary to PV and ET prognostic model [MYSEC]), disease stage (chronic, accelerated), and diagnoses (primary MF, post–polycythemia vera MF, and post–essential thrombocythemia MF) of the respective patient sample (supplemental Figure 3A-C).

Furthermore, both mouse strains supported predominantly human myeloid ($CD33^+$) engraftment in all organs analyzed (Figure 1D-E). Next, because monocytosis and the presence of myeloid progenitors in the PB are typical features of MF, we examined human monocytic ($CD33^+CD14^+$) and myeloid progenitor ($CD33^+CD34^+$) development in the PDXs (Figure 1F).[28] As expected, the proportion of myeloid progenitors was higher in the BM than in the PB, whereas the fraction of monocytes was higher in the PB. A myeloid population negative for CD14 and CD34 was found in all organs analyzed. This cell fraction contained a significant proportion of granulated myeloid cells based on CD33 expression and side scatter, which suggested the development of human granulocytes in both mouse strains (Figure 1D; supplemental Figure 4A). The presence of human neutrophil granulocytes was further confirmed by purification and morphological analysis of human $SSC^{hi}CD33^+CD15^+CD14^-CD34^-$ cells from the BM of engrafted MISTRG mice (supplemental Figure 4B-E). Megakaryocytic proliferation in clusters and morphological atypia are hallmarks of MF.[29] IHC analysis of BM sections from mice that displayed ≥10% total human engraftment revealed the development of human megakaryocytes in both mouse strains (Figure 2A). However, because of the higher proportion of engrafting MISTRG mice and the higher total engraftment level, megakaryocyte development could be assessed for more patient samples using MISTRG mice (supplemental Figure 5A). We then compared the morphology of engrafted human megakaryocytes ($CD61^+$) between MISTRG mice transplanted with a healthy BM donor sample to MISTRG engrafted with human MF patient samples. MISTRG mice supported the development of megakaryocytes with typical MPN features resembling the megakaryocytes in the respective patient BM section (Figure 2B). Also, formation of megakaryocyte clusters was observed (supplemental Figure 5B-C). This shows that megakaryocyte development in MISTRG mice mimics morphological atypia observed in MF patients.

Another characteristic feature of MF is the deposition of reticulin and collagen fibers in the BM. We assessed reticulin fiber formation in mice with ≥10% human engraftment (Figure 2B; supplemental Figure 5D). Fibrosis grade 1, according to WHO criteria, was observed in MISTRG mice transplanted with 3 patient samples but not in any of the NSG mice. However, even within 1 group of MISTRG mice transplanted with the same patient sample, fibrosis development was limited to a minority of mice (1 of 3, 1 of 3, 2 of 6 mice). In summary, human MF engraftment in MISTRG mice is significantly enhanced in comparison with NSG mice. Both NSG and MISTRG mice promote myeloid MF differentiation and development of atypical human megakaryocytes, whereas the development of reticulin fibrosis is a rare event in MISTRG mice.

MF results from disease-initiating driver mutations in HSCs, followed by the acquisition of additional somatic mutations, which can contribute to disease progression. Typically, MF patients carry 1 to 4 somatic mutations.[11] To determine whether the engrafted human cells were derived from the MF clone, we analyzed NSG and MISTRG mice with ≥10% human engraftment for the presence of driver mutations (supplemental Table 4). *JAK2*-V617F and *CALR* mutations were detected in all xenografts transplanted with the respective patient samples, which shows the presence of MF hematopoiesis in all investigated mice.

To determine whether the driver and additional somatic mutations found in the $CD34^+$ fraction of the original patient sample were preserved in MISTRG mice, we performed targeted sequencing on xenografts derived from 8 patient samples (Figure 3). Overall, MISTRG mice captured the mutations present in the injected $CD34^+$ fraction of 7 of 8 patient samples. However, in sample 8, the

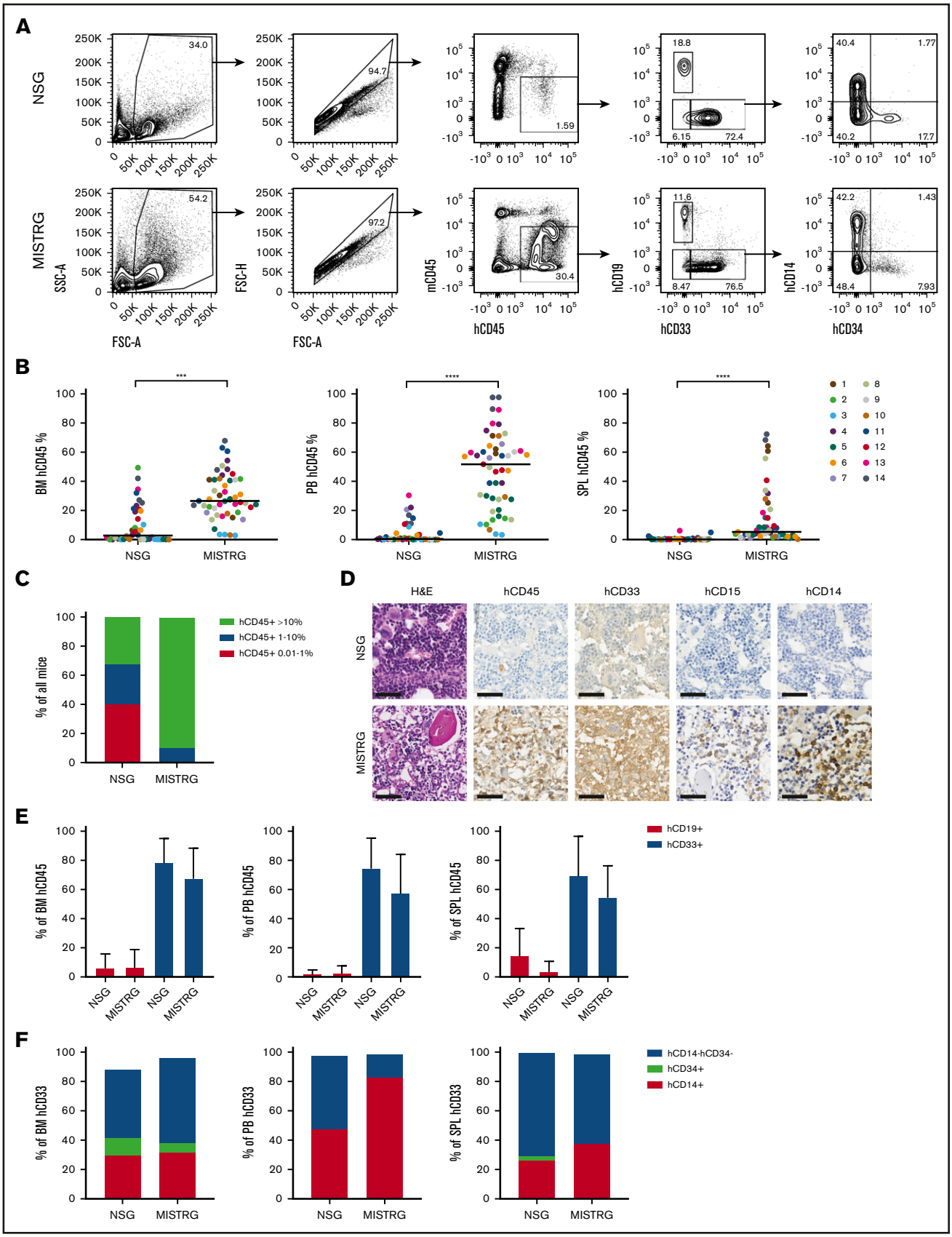

Figure 1.

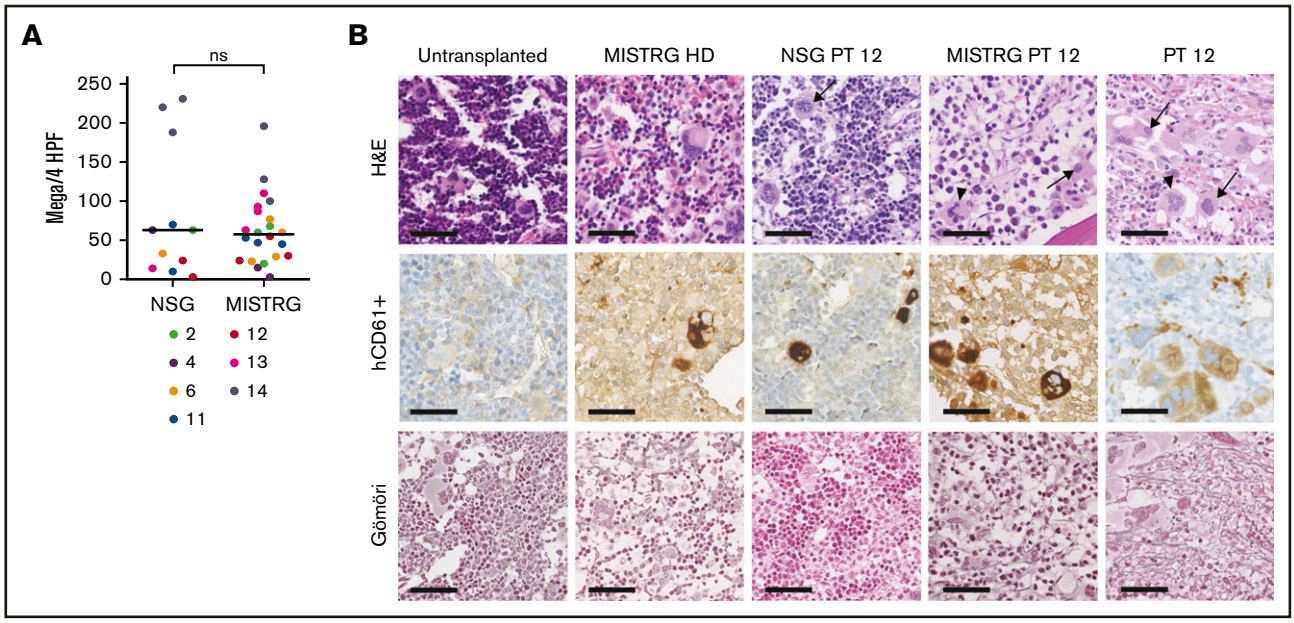

Figure 2. Immunohistochemical analysis of MF engrafted NSG and MISTRG mice BM. (A) Number of human megakaryocytes (Mega, $CD61^+$) per 4 high power fields (HPF, equaling 1 mm^2) in NSG and MISTRG mice for patient (PT) samples with ≥10% $hCD45^+$ (grand median, unpaired Student *t* test). (B) Representative IHC analysis for hCD61 and Gömöri (stains reticulin fibers) of the BM of an untransplanted MISTRG mouse, a MISTRG mouse transplanted with a healthy donor sample (HD), a NSG and a MISTRG mouse transplanted with sample from a post–essential thrombocythemia patient (PT 12), and the BM biopsy from the same patient (scale bars, 50 μm; original magnification ×400). Arrows point to atypical human MF megakaryocytes. Arrowheads point to atypical human ET megakaryocytes. ns, not significant.

VAF of *JAK2*-V617F and other mutations was significantly lower in MISTRG mice compared with the patient $CD34^+$ fraction. Because healthy unmutated HSPCs can be present within the $CD34^+$ fraction of MF patients, we reasoned that the lower VAF in the xenografts transplanted with this patient sample might represent normal human engraftment.[30] Myeloid cells carried the *JAK2* mutation in the patient sample, but not B cells. In contrast, myeloid cells purified from the BM of MISTRG mice carried a much lower mutant allele burden of *JAK2* (supplemental Figure 6). This shows that *JAK2* unmutated HSPCs engrafted MISTRG mice, which is compatible with the development of normal functional hematopoiesis derived from the patient $CD34^+$ fraction. Furthermore, mutations in *CALR* and *CUX1* with low allele frequency newly appeared in mice transplanted with the same patient sample. These mutations possibly reflect the expansion of rare subclones present below the detection limit or de novo acquisition in this sample. In patient sample 13, the VAF for the *JAK2* and the *TP53* mutation was higher in MISTRG mice compared with the patient $CD34^+$ fraction. The microarray analysis performed previously on the patient BM revealed loss of heterozygosity on chromosome 9p and deletion of chromosome 17p, which explains a VAF >50% in the patient (data not shown). Therefore, the increased VAF of both mutations in MISTRG mice can be explained by an expansion of the double-mutated clone found in the patient $CD34^+$ fraction. In conclusion, our data show the maintenance of the mutational architecture of the primary patient samples in the corresponding MISTRG xenografts mice in the majority of cases. It further demonstrates that the comparison of the clonal composition of the patient sample with the respective xenografts can reveal the development of presumably normal human hematopoiesis and clonal expansion in mice.

Next, we assessed the repopulation capacity of human MF stem cells (SCs) engrafted in MISTRG mice. Purified $hCD45^+$ cells from 5 primary MISTRG mice from 3 patient samples (10, 11, and 13) with a detectable human MF SC fraction ($CD34^+CD38^-$) were transplanted into 6 secondary recipients (Figure 4A-B). Overall, the total human engraftment in secondary MISTRG mice was significantly lower than in the respective primary mice (Figure 4C; supplemental Figure 7; supplemental Table 3). The human BM, PB, and SPL engraftment was higher in secondary mice transplanted with patient samples 11 and 13 compared with patient sample 10, which correlated with the size of the MF SC fraction in primary MISTRG mice. Finally, as in primary mice, the engrafted human cells

Figure 1. Human MF engraftment in NSG and MISTRG mice. (A) Scatter plots depicting total human engraftment ($hCD45^+$) and lineage distribution. (B) Total human engraftment of 14 MF samples in the BM, PB, and SPL of NSG and MISTRG mice. Each dot represents an individual mouse and each color represents an individual patient. (C) Percentage of NSG and MISTRG mice with human BM engraftment levels as indicated. (D) Representative H&E and immunohistochemical (IHC) photomicrographs for hCD45, hCD33, hCD15, and hCD14 of the BM of an NSG and MISTRG mice transplanted with the same patient sample (patient 1) (scale bars, 50 μm; original magnification ×400). (E) Relative contribution of human B-lymphoid and myeloid cells to the total human engraftment in the BM, PB, and SPL of NSG and MISTRG mice. (F) Relative contribution of monocytes ($CD14^+CD34^-$), hematopoietic stem and progenitor cells ($CD14^-CD34^+$), and other cells ($CD14^-CD34^-$) to total human myeloid cells in the BM, PB, and SPL. Results are represented as grand median (B-C,F) and mean ± standard deviation (E). ***$P < .001$; ****$P < .0001$ (Mann-Whitney *U* test). FSC-A, forward scatter area; SSC-A, side scatter area; FSC-H, forward scatter height.

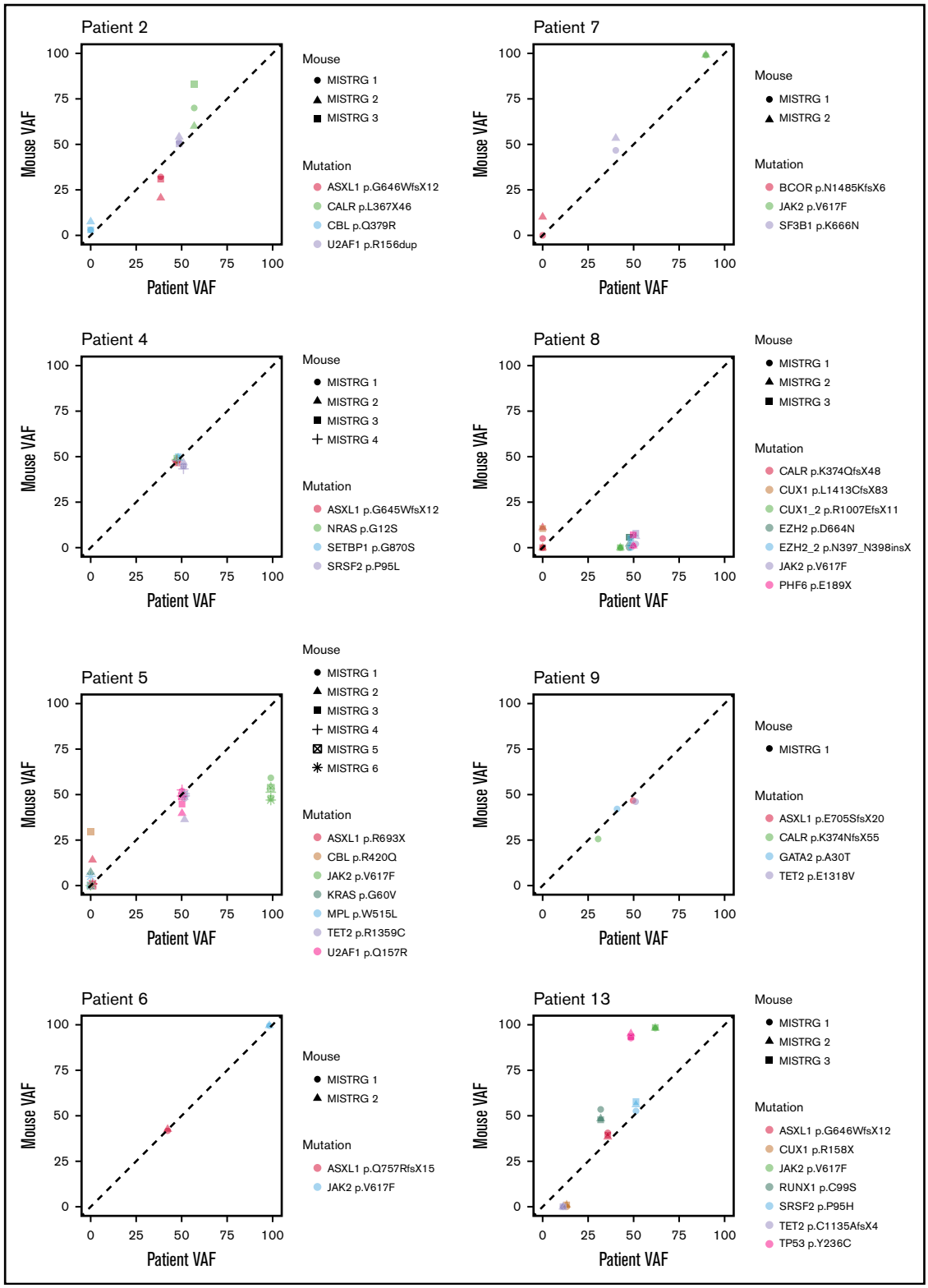

Figure 3. Mutational landscape in MF MISTRG xenografts. Variant allele frequency (VAF) of somatic mutations found by targeted sequencing of CD34$^+$ cells from 8 patient samples and the BM of the respective MISTRG xenografts. Each symbol represents 1 mouse, and each color represents a mutation as indicated.

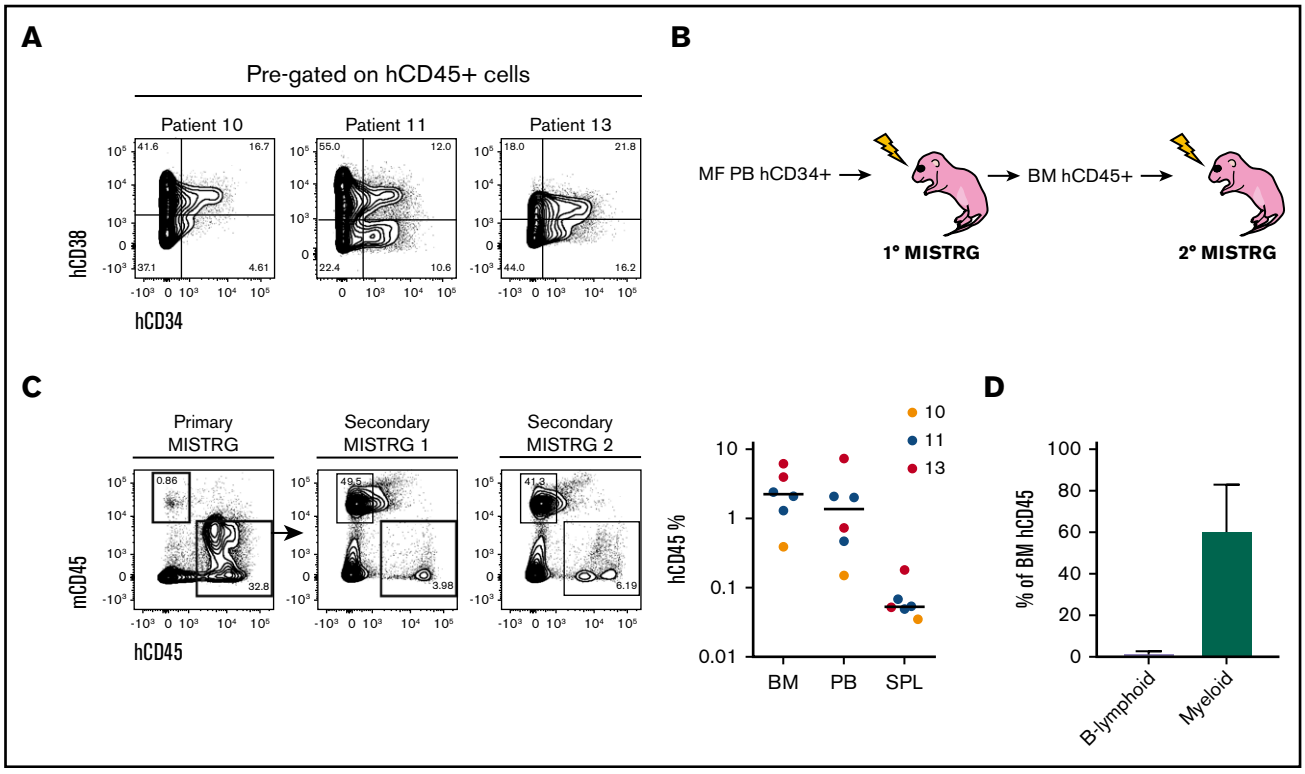

Figure 4. Characterization of MF HSPCs and serial repopulation analysis. (A) Representative flow cytometry plots of the human stem (hCD34$^+$hCD38$^-$) and progenitor (hCD34$^+$hCD38$^+$) cell fraction out of total hCD45$^+$ cells from 3 MISTRG mice transplanted with 3 different samples (10, 11, and 13). (B) Workflow for serial transplantation of purified hCD45$^+$ cells from primary into secondary MISTRG mice. (C, left) Flow cytometry plots of primary and secondary MISTRG mice from sample 13, 9.7 weeks (primary MISTRG) and 17.9 weeks (secondary MISTRG) post-transplantation, respectively. (C, right) Total human engraftment in the BM, PB, and SPL of secondary MISTRG recipients. Each dot represents an individual mouse; each color represents an individual patient. (D) Distribution of human B-lymphoid and myeloid lineages. Results are expressed as mean ± standard deviation.

were mainly from the myeloid lineage (Figure 4D). The data demonstrate that MISTRG mice support low-level secondary repopulation of MF SC and that the CD34$^+$CD38$^-$ fraction contains MF repopulating cells.

The JAKi Rux was the first approved targeted therapy for MF.[13] We next examined the effect of Rux in the MISTRG MF PDX model. Rux was administered for 21 days in mice with >5% human engraftment in the PB 4 weeks after transplantation (Figure 5A). We observed a moderate but significant reduction in human engraftment in the PB and the BM, which correlated with a reduced SPL size in Rux-treated mice (Figure 5B-C). However, the human engraftment in the SPL was not affected by Rux treatment. Regardless of treatment, mice developed pancytopenia, and human engraftment was predominantly myeloid in the BM, PB, and SPL (Figure 5D; supplemental Figure 8). The data show that Rux can be administered to MISTRG MF PDX mice and it reduces human engraftment and SPL weight. Pancytopenia was likely the consequence of human MF engraftment and not of Rux treatment, because no difference in complete blood counts was observed between the Rux and control groups.

Discussion

MF is an HSPC neoplasm that has been challenging to recapitulate in PDX models. In this study, we demonstrate that MISTRG mice, which produce human M-CSF, IL-3, GM-CSF, TPO, and express human SIRPα, support unprecedented human engraftment in comparison with the widely used NSG mouse strain. In particular, MISTRG mice allowed the assessment of more MF patient samples than NSG mice, which will be relevant for testing candidate therapeutic compounds without generating a selection bias. We observed human engraftment in MISTRG mice in all patient samples investigated, although most patients were exposed to treatment with the JAKi Rux at the time of sampling. This shows that at least a fraction of MF HSPCs retains MISTRG repopulation potential in the presence of Rux. The engraftment of MF patient samples in PDX did not correlate with established MF prognostic scores, including MIPSS70 and MYSEC-PM, which integrate molecular testing. However, additional cell-intrinsic and extrinsic factors may contribute to MF HSPC development in MISTRG mice. Our comparison with *Rag2*$^{-/-}$*Il2rγ*$^{-/-}$ mice with a limited number of samples suggests a strong dependence of human MF SCs on human cytokines and the CD47-SIRPα interaction. NSG mice express a SIRPα variant that closely resembles human SIRPα and binds human CD47 with high affinity, which may explain the enhanced engraftment potential in comparison with *Rag2*$^{-/-}$*Il2rγ*$^{-/-}$ mice.[22] The presence of human cytokines likely further potentiates human MF engraftment in MISTRG mice. The data also correlate with the increased expression of the receptors for IL-3, GM-CSF, and CD47 observed in MF patient granulocytes and suggest that MF hematopoiesis may particularly benefit from these interactions in vivo. This observation is also in line with a recent report that demonstrates the M-CSF-dependence of AML with inv(16) in

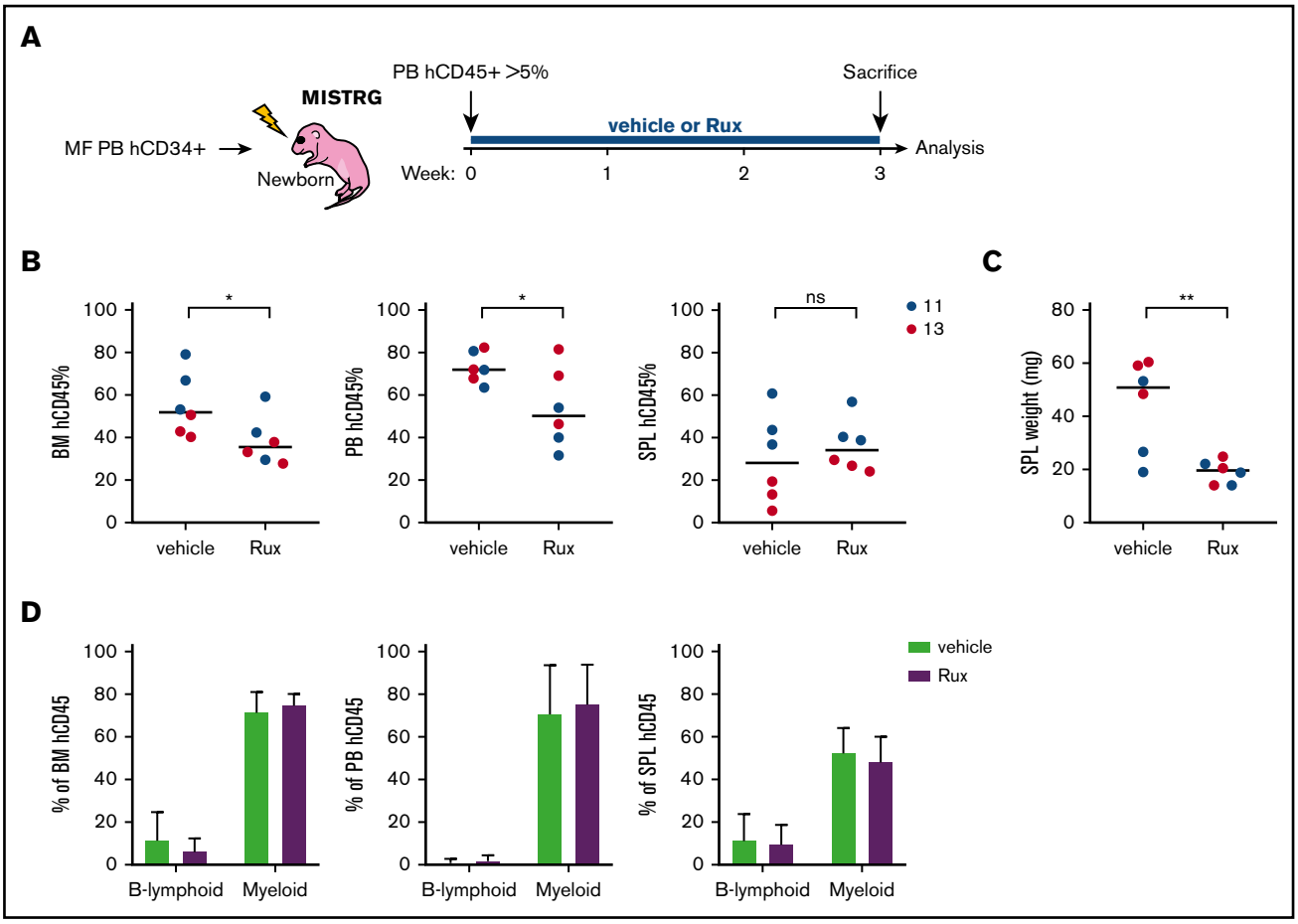

Figure 5. Rux treatment in the MISTRG MF PDX model. (A) Workflow of the experimental treatment plan with control (vehicle) or Rux. (B) Total human engraftment in the BM, PB, and SPL of MISTRG mice 21 days after treatment with vehicle or Rux. (C) SPL weight of MISTRG mice 21 days after treatment with vehicle or Rux. (D) Percentage of human B-lymphoid and myeloid cells among total engrafted human cells in the BM, PB, and SPL after vehicle or Rux treatment. *$P < .05$; **$P < .01$ (unpaired Student t test).

MISTRG mice due to overexpression of the M-CSF receptor on AML blasts.[24] The identification of cytokine dependence in vivo may represent disease vulnerabilities that could be exploited therapeutically. Also, targeting CD47 in advanced aggressive lymphoma has demonstrated significant efficacy in combination with Rituximab in recent clinical trials, and several trials investigate the value of targeting CD47 in MDS and AML.[31,32]

Although we observed low-grade reticulin fibrosis in a limited number of mice, our model does not support robust and consistent development of this process. The interplay between dysplastic megakaryocytes, inflammatory cytokines, and extracellular matrix producing cells drive the fibrotic process in MF. The lack of consistent fibrosis development could be due to insufficient cross-reactivity between factors secreted by human MF megakaryocytes and the mouse stroma. Indeed, the induction of an aberrant stroma by MF cells contributes to the fibrotic process in MPN.[33,34] Human transforming growth factor β1 (TGFβ1) is an essential factor for fibrosis development.[35] Leptin-receptor–positive and Gli1$^+$ mesenchymal stromal cells transform into fibrosis-driving cells through stimulation by platelet-derived growth factor α (PDGFα) and CXC chemokine ligand 4 (CXCL4), secreted by megakaryocytes.[34,36,37] The sequence homology between mouse and human for TGFβ1 (89.7%) and PDGFα (92.4%) is high, supporting cross-reactivity with the mouse stroma.[21] However, the sequence homology for CXCL4 is lower (67.6%), possibly limiting the fibrotic transformation of the BM in PDX models. Besides cytokines and direct cell-cell interactions, the development of BM fibrosis is also dependent on time and the number of MF megakaryocytes. In humans, BM fibrosis is a process that develops over the years, whereas in MPN mouse models, the expression of an MF driver mutation leads to fibrosis after at least 28 to 32 weeks in some, but not all models.[38-41] In our model, the observation period ranged from 3.6 to 19.7 weeks. Therefore, another limiting factor could be the relatively short observation period in this work. In our cohort, we also describe MF PDX mice with up to 200 dysplastic megakaryocytes per high power field (eg, patient sample 14) without concomitant fibrosis, implying that the number of megakaryocytes itself is not the only restricting factor. This indicates that additional factors preclude consistent fibrosis development in PDX mice. Recently, the engraftment potential of human fetal liver CD34$^+$ cells was compared between NSG mice with a *Kit* mutation (NSGW41) and MISTRG mice.[42] Both mouse strains showed similar engraftment potential and lineage distribution. It would be of interest to assess the development potential of human MF in NSGW41 mice in future studies with a particular focus on fibrosis development.

Capturing the clonal composition of a patient in vivo is essential for potentially testing novel targeted therapies that possess disease-modifying potential and act at the clonal level. Our work captures MF clones in vivo at the clonal and subclonal level. We show maintenance of the mutational profile in almost 90% of primary MF samples in MISTRG PDX mice, which supports the use of the model in preclinical drug testing to identify compounds that target and affect the MF clone. Recent studies further dissected the MF SC compartment at the single-cell level.[30,43] These studies revealed significant heterogeneity at the clonal level. In particular, normal cells were detected in the HSC fraction, which may explain the engraftment of normal human hematopoiesis in MISTRG mice, as observed with 1 patient sample in this study.

Immunocompromised mouse strains have been essential to defining human HSCs functionality.[44] Although phenotypic assessment of MF HSPCs determines their presence, secondary repopulation experiments are critical to test their functionality. A previous study using humanized ossicles has shown that MF repopulating cells reside exclusively in the $CD34^+CD38^-$ compartment, but secondary repopulation has not been investigated.[19] In this study, we show that only mice with a robust $CD34^+CD38^-$ fraction in primary MISTRG mice have repopulating capacity in secondary animals.

Finally, we examined the effect of the JAKi Rux in the MISTRG MF PDX model. The inhibition of JAK signaling significantly reduced human engraftment in the BM and PB, but not in the SPL, although SPL weight was significantly reduced. Splenic enlargement in PDX mice is often the consequence of increased extramedullary murine hematopoiesis in order to compensate for reduced BM production due to the expansion of human cells.[45] We hypothesize that the reduction of splenomegaly is at least partly due to a reduction of the human graft in the BM, which likely leads to re-expansion of murine BM hematopoiesis. JAK inhibition could also indirectly affect human MF HSPC development by limiting the support of human cytokines dependent on JAK-STAT signaling and provided by the mouse environment. This is an observation that would further underline the dependence of MF HSPCs on the humanized murine BM niche.[46] The MF PDX model will be a valuable tool to assess the effects of compounds on the MF HSPC compartment. Based on our findings, with only a modest reduction of the human MF engraft in Rux-treated mice and the marginally affected mutant allele burden in the majority of Rux-treated patients, we postulate that Rux treatment has little functional impact on MF HSPCs. Future studies in the MF PDX model will allow identifying compounds that affect the secondary repopulation potential of MF HSPCs. The elimination of MF HSPCs may eventually lead to the regression of fibrosis, as observed in patients treated with allo-HSCT.[47,48]

In summary, MISTRG mice support robust engraftment of MF HSPCs and preserve the genetic heterogeneity of the patient MF driving cells. These similarities render the MF PDX model valuable for dissecting disease pathogenesis and assessing established and novel therapeutic agents in an individualized patient-specific approach.

Acknowledgments

The authors thank Yvonne Fuhrer, Andrina Julia Stäubli, Ewerton Marques Maggio, Fabiola Prutek, and Susanne Dettwiler for technical assistance.

This work was supported by the Swiss Cancer League (KLS-3298-08-2013) (A.P.A.T.). A.P.A.T. is supported by the Professor Dr. Max Cloëtta Foundation. V.L. is a recipient of a Forschungskredit fellowship from the University of Zurich. Funding was also provided by the University of Zurich Clinical Research Priority Program "Human Hemato-Lymphatic Diseases" (M.G.M.) and the Novartis Foundation for Medical-Biological Research (A.P.A.T.). A.M.V. and L.C. were supported by the Istituto Toscano Tumori, Regione Toscana, project 2013-B16D14001130002; AIRC 5x1000 call "Metastatic disease: the key unmet need in oncology" to MYNERVA project, #21267 (MYeloid NEoplasms Research Venture AIRC); and by the "EDITOR" Accelerator Award project, funded through a partnership between Cancer Research UK, Fondazione AIRC, and Fundación Científica de la Asociacion Española Contra el Cáncer.

Authorship

Contribution: V.L. designed and performed research, analyzed data, and wrote the paper; N.W.-V.v.W., K.Z., M.-C.W., M.B., M.H.E.W., P.S., C.F., U.W., and L.C. performed research and analyzed data; B.P., R.A.F., A.M.V., A.J.M., P.J.W., and S.D. analyzed data; M.G.M. and A.P.A.T. designed research, analyzed data, and wrote the paper; and A.P.A.T. directed the studies.

Conflict-of-interest disclosure: The authors declare no competing financial interests.

ORCID profiles: M.H.E.W., 0000-0002-6460-3084; P.S., 0000-0003-3895-2149; B.P., 0000-0001-8198-9663; R.A.F., 0000-0003-4461-0778; A.M.V., 0000-0001-5755-0730; P.J.W., 0000-0002-1017-3744; A.P.A.T., 0000-0002-1535-8692.

Correspondence: Alexandre P. A. Theocharides, Department of Medical Oncology and Hematology, University Hospital Zurich, Raemistr 100, CH-8091 Zurich, Switzerland; e-mail alexandre.theocharides@usz.ch.

References

1. Arber DA, Orazi A, Hasserjian R, et al. The 2016 revision to the World Health Organization classification of myeloid neoplasms and acute leukemia. *Blood*. 2016;127(20):2391-2405.
2. Barbui T, Carobbio A, Cervantes F, et al. Thrombosis in primary myelofibrosis: incidence and risk factors. *Blood*. 2010;115(4):778-782.
3. Vallapureddy RR, Mudireddy M, Penna D, et al. Leukemic transformation among 1306 patients with primary myelofibrosis: risk factors and development of a predictive model. *Blood Cancer J*. 2019;9(2):12.
4. James C, Ugo V, Le Couédic JP, et al. A unique clonal JAK2 mutation leading to constitutive signalling causes polycythaemia vera. *Nature*. 2005;434(7037):1144-1148.

5. Levine RL, Wadleigh M, Cools J, et al. Activating mutation in the tyrosine kinase JAK2 in polycythemia vera, essential thrombocythemia, and myeloid metaplasia with myelofibrosis. *Cancer Cell*. 2005;7(4):387-397.
6. Kralovics R, Passamonti F, Buser AS, et al. A gain-of-function mutation of JAK2 in myeloproliferative disorders. *N Engl J Med*. 2005;352(17):1779-1790.
7. Baxter EJ, Scott LM, Campbell PJ, et al; Cancer Genome Project. Acquired mutation of the tyrosine kinase JAK2 in human myeloproliferative disorders. *Lancet*. 2005;365(9464):1054-1061.
8. Pikman Y, Lee BH, Mercher T, et al. MPLW515L is a novel somatic activating mutation in myelofibrosis with myeloid metaplasia. *PLoS Med*. 2006;3(7):e270.
9. Klampfl T, Gisslinger H, Harutyunyan AS, et al. Somatic mutations of calreticulin in myeloproliferative neoplasms. *N Engl J Med*. 2013;369(25):2379-2390.
10. Nangalia J, Massie CE, Baxter EJ, et al. Somatic CALR mutations in myeloproliferative neoplasms with nonmutated JAK2. *N Engl J Med*. 2013;369(25):2391-2405.
11. Lundberg P, Karow A, Nienhold R, et al. Clonal evolution and clinical correlates of somatic mutations in myeloproliferative neoplasms. *Blood*. 2014;123(14):2220-2228.
12. Mesa RA, Kiladjian JJ, Verstovsek S, et al. Comparison of placebo and best available therapy for the treatment of myelofibrosis in the phase 3 COMFORT studies. *Haematologica*. 2014;99(2):292-298.
13. Ganetsky A. Ruxolitinib: a new treatment option for myelofibrosis. *Pharmacotherapy*. 2013;33(1):84-92.
14. Gupta V, Gotlib J, Radich JP, et al. Janus kinase inhibitors and allogeneic stem cell transplantation for myelofibrosis. *Biol Blood Marrow Transplant*. 2014;20(9):1274-1281.
15. Morotti A, Rocca S, Carrà G, Saglio G, Brancaccio M. Modeling myeloproliferative neoplasms: from mutations to mouse models and back again. *Blood Rev*. 2017;31(3):139-150.
16. Theocharides AP, Rongvaux A, Fritsch K, Flavell RA, Manz MG. Humanized hemato-lymphoid system mice. *Haematologica*. 2016;101(1):5-19.
17. Wang X, Prakash S, Lu M, et al. Spleens of myelofibrosis patients contain malignant hematopoietic stem cells. *J Clin Invest*. 2012;122(11):3888-3899.
18. Verstovsek S, Manshouri T, Pilling D, et al. Role of neoplastic monocyte-derived fibrocytes in primary myelofibrosis. *J Exp Med*. 2016;213(9):1723-1740.
19. Reinisch A, Thomas D, Corces MR, et al. A humanized bone marrow ossicle xenotransplantation model enables improved engraftment of healthy and leukemic human hematopoietic cells. *Nat Med*. 2016;22(7):812-821.
20. Rongvaux A, Willinger T, Martinek J, et al. Development and function of human innate immune cells in a humanized mouse model [published correction appears in *Nat Biotechnol*. 2017;35(12):1211.]. *Nat Biotechnol*. 2014;32(4):364-372.
21. Rongvaux A, Takizawa H, Strowig T, et al. Human hemato-lymphoid system mice: current use and future potential for medicine. *Annu Rev Immunol*. 2013;31(1):635-674.
22. Takenaka K, Prasolava TK, Wang JC, et al. Polymorphism in Sirpa modulates engraftment of human hematopoietic stem cells. *Nat Immunol*. 2007;8(12):1313-1323.
23. Song Y, Rongvaux A, Taylor A, et al. A highly efficient and faithful MDS patient-derived xenotransplantation model for pre-clinical studies. *Nat Commun*. 2019;10(1):366.
24. Ellegast JM, Rauch PJ, Kovtonyuk LV, et al. inv(16) and NPM1mut AMLs engraft human cytokine knock-in mice. *Blood*. 2016;128(17):2130-2134.
25. Deng K, Pertea M, Rongvaux A, et al. Broad CTL response is required to clear latent HIV-1 due to dominance of escape mutations. *Nature*. 2015;517(7534):381-385.
26. Tso KY, Lee SD, Lo KW, Yip KY. Are special read alignment strategies necessary and cost-effective when handling sequencing reads from patient-derived tumor xenografts? *BMC Genomics*. 2014;15(1):1172.
27. Rampal R, Al-Shahrour F, Abdel-Wahab O, et al. Integrated genomic analysis illustrates the central role of JAK-STAT pathway activation in myeloproliferative neoplasm pathogenesis. *Blood*. 2014;123(22):e123-e133.
28. Barosi G, Viarengo G, Pecci A, et al. Diagnostic and clinical relevance of the number of circulating CD34(+) cells in myelofibrosis with myeloid metaplasia. *Blood*. 2001;98(12):3249-3255.
29. Thiele J, Kvasnicka HM, Orazi A. Bone marrow histopathology in myeloproliferative disorders–current diagnostic approach. *Semin Hematol*. 2005;42(4):184-195.
30. Rodriguez-Meira A, Buck G, Clark SA, et al. Unravelling intratumoral heterogeneity through high-sensitivity single-cell mutational analysis and parallel RNA sequencing. *Mol Cell*. 2019;73(6):1292-1305.
31. Weiskopf K. Cancer immunotherapy targeting the CD47/SIRPα axis. *Eur J Cancer*. 2017;76:100-109.
32. Advani R, Flinn I, Popplewell L, et al. CD47 blockade by Hu5F9-G4 and rituximab in non-Hodgkin's lymphoma. *N Engl J Med*. 2018;379(18):1711-1721.
33. Reynaud D, Pietras E, Barry-Holson K, et al. IL-6 controls leukemic multipotent progenitor cell fate and contributes to chronic myelogenous leukemia development. *Cancer Cell*. 2011;20(5):661-673.
34. Schneider RK, Mullally A, Dugourd A, et al. Gli1(+) mesenchymal stromal cells are a key driver of bone marrow fibrosis and an important cellular therapeutic target. *Cell Stem Cell*. 2017;20(6):785-800.
35. Chagraoui H, Komura E, Tulliez M, Giraudier S, Vainchenker W, Wendling F. Prominent role of TGF-beta 1 in thrombopoietin-induced myelofibrosis in mice. *Blood*. 2002;100(10):3495-3503.

36. Zhou BO, Yue R, Murphy MM, Peyer JG, Morrison SJ. Leptin-receptor-expressing mesenchymal stromal cells represent the main source of bone formed by adult bone marrow. *Cell Stem Cell*. 2014;15(2):154-168.

37. Decker M, Martinez-Morentin L, Wang G, et al. Leptin-receptor-expressing bone marrow stromal cells are myofibroblasts in primary myelofibrosis. *Nat Cell Biol*. 2017;19(6):677-688.

38. Kubovcakova L, Lundberg P, Grisouard J, et al. Differential effects of hydroxyurea and INC424 on mutant allele burden and myeloproliferative phenotype in a JAK2-V617F polycythemia vera mouse model. *Blood*. 2013;121(7):1188-1199.

39. Shide K, Kameda T, Yamaji T, et al. Calreticulin mutant mice develop essential thrombocythemia that is ameliorated by the JAK inhibitor ruxolitinib. *Leukemia*. 2017;31(5):1136-1144.

40. Shide K, Kameda T, Kamiunten A, et al. Mice with Calr mutations homologous to human CALR mutations only exhibit mild thrombocytosis. *Blood Cancer J*. 2019;9(4):42.

41. Li J, Prins D, Park HJ, et al. Mutant calreticulin knockin mice develop thrombocytosis and myelofibrosis without a stem cell self-renewal advantage. *Blood*. 2018;131(6):649-661.

42. Sippel TR, Radtke S, Olsen TM, Kiem HP, Rongvaux A. Human hematopoietic stem cell maintenance and myeloid cell development in next-generation humanized mouse models. *Blood Adv*. 2019;3(3):268-274.

43. Nam AS, Kim K-T, Chaligne R, et al. Somatic mutations and cell identity linked by genotyping of transcriptomes. *Nature*. 2019;571(7765):355-360.

44. Doulatov S, Notta F, Laurenti E, Dick JE. Hematopoiesis: a human perspective. *Cell Stem Cell*. 2012;10(2):120-136.

45. Saito Y, Ellegast JM, Rafiei A, et al. Peripheral blood $CD34^{+}$ cells efficiently engraft human cytokine knock-in mice. *Blood*. 2016;128(14):1829-1833.

46. O'Sullivan LA, Liongue C, Lewis RS, Stephenson SE, Ward AC. Cytokine receptor signaling through the Jak-Stat-Socs pathway in disease. *Mol Immunol*. 2007;44(10):2497-2506.

47. Kröger N, Thiele J, Zander A, et al; MDS-Subcommittee of the Chronic Leukaemia Working Party of the European Group for Blood and Marrow Transplantation. Rapid regression of bone marrow fibrosis after dose-reduced allogeneic stem cell transplantation in patients with primary myelofibrosis. *Exp Hematol*. 2007;35(11):1719-1722.

48. Kröger N, Zabelina T, Alchalby H, et al. Dynamic of bone marrow fibrosis regression predicts survival after allogeneic stem cell transplantation for myelofibrosis. *Biol Blood Marrow Transplant*. 2014;20(6):812-815.